Molecular Therapy
Oncolytics
Review

Toward comprehensive imaging of oncolytic viroimmunotherapy

Shyambabu Chaurasiya,[1,3] Sang-In Kim,[1,3] Michael O'Leary,[1] Anthony K. Park,[2] Jianming Lu,[1] Seonah Kang,[1] Zhifang Zhang,[1] Annie Yang,[1] Yanghee Woo,[1] Yuman Fong,[1] and Susanne G. Warner[1]

[1]Department of Surgery, Division of Surgical Oncology, City of Hope National Medical Center, 1500 East Duarte Road, Pavilion 2226, Duarte, CA 91010, USA; [2]Center for Gene Therapy, Department of Hematologic and Hematopoietic Cell Transplantation, Beckman Research Institute, City of Hope National Medical Center, Duarte, CA 91010, USA

Oncolytic viruses infect, replicate in, and kill cancer cells, leaving normal cells unharmed; they also recruit and activate immune cells against tumor cells. While clinical indications for viroimmunotherapy are growing, barriers to widespread treatment remain. Ensuring real-time tracking of viral replication and resulting anti-tumor immune responses will overcome some of these barriers and is thus a top priority. Clinically optimizing trackability of viral replication will promote safe dose increases, guide serial dosing, and enhance treatment effects. However, viral delivery is only half the story. Oncolytic viruses are known to upregulate immune checkpoint expression, thereby priming otherwise immunodeficient tumor immune microenvironments for treatment with checkpoint inhibitors. Novel modalities to track virus-induced changes in tumor microenvironments include non-invasive measurements of immune cell populations and responses to viroimmunotherapy such as (1) *in situ* use of radiotracers to track checkpoint protein expression or immune cell traffic, and (2) *ex vivo* labeling of immune cells followed by nuclear medicine imaging. Herein, we review clinical progress toward accurate imaging of oncolytic virus replication, and we further review the current status of functional imaging of immune responses to viroimmunotherapy.

INTRODUCTION

Oncolytic viruses (OVs) are a powerful tool of immunogenicity and are capable of conferring anti-tumor immunity even to disseminated cancers. While one virus is currently US Food and Drug Administration (FDA)-approved for melanoma treatment, barriers remain to the widespread use of viroimmunotherapy in solid tumor treatment algorithms. With an average time to response of approximately 4 months as seen in the OPTIM trial prompting talimogene laherparepvec (T-Vec) approval,[1–3] oncolytic virologists and medical oncologists alike are left to guess whether continued OV or other cancer treatment dosing will benefit the patient. This is especially harrowing in the setting of pseudo-progression or progression prior to response, which can occur in up to 49% of responders.[4,5] In many cases, we simply continue to treat until a tumor marker rises, or an image demonstrates definitive tumor progression, unaware whether we have benefited the patient with the preceding months of therapy. The inability to non-invasively measure treatment progress in real time is a barrier shared by OVs, immunotherapies, and traditional cytotoxic treatments alike. Non-invasive diagnostics that can provide valid feedback would save money, time, and toxicity for many.

Attempts at optimizing clinical imaging of viral replication in tumors have been ongoing during the last 20 years with limited success.[6] Real-time imaging allows OVs to meet their full theranostic potential. Indeed, many OVs currently in clinical testing accommodate transgenes encoding "payloads" that include enhancement of immunogenicity and also reporter genes that allow for real-time tracking of viral replication. Given that many OVs are tumor-tropic, viral imaging may elucidate previously undetected tumors. Ultimately, imaging of OV trafficking and viability could yield truly personalized medicine by guiding variables such as future serial injections for intratumoral models and dose increases for systemic delivery. However, despite years of clinical development spanning disease and vector types, optimal dose timing and the best vector and dosing strategy for each specific tumor remain a challenge.[7]

Thus far, there are two predominant types of real-time OV imaging: optical and deep tissue functional imaging. Clinically, optical imaging allows direct visualization of fluorescence. In the operating room, special laparoscopes can elucidate fluorescent tissue within body cavities. In the clinic, lamps can reveal fluorescent epidermal or mucosal surfaces.[8] Functional viral imaging measures isotope uptake as a surrogate for viral replication with scans such as positron emission tomography (PET) or single-photon emission computed tomography (SPECT). Of the reporter genes in OV clinical trials, human sodium iodide symporter (hNIS) is the most prominent.[9] However, only a selected few investigators have published actual human images.[8,10–15]

While critical to the success of the field, tracking viral delivery is only half the story. Reliable non-invasive characterization of virally

https://doi.org/10.1016/j.omto.2021.06.010.

[3]These authors contributed equally

Correspondence: Susanne G. Warner, MD, Department of Surgery, Division of Surgical Oncology, City of Hope National Medical Center, 1500 East Duarte Road, Pavilion 2226, Duarte, CA 91010, USA.
E-mail: suwarner@coh.org

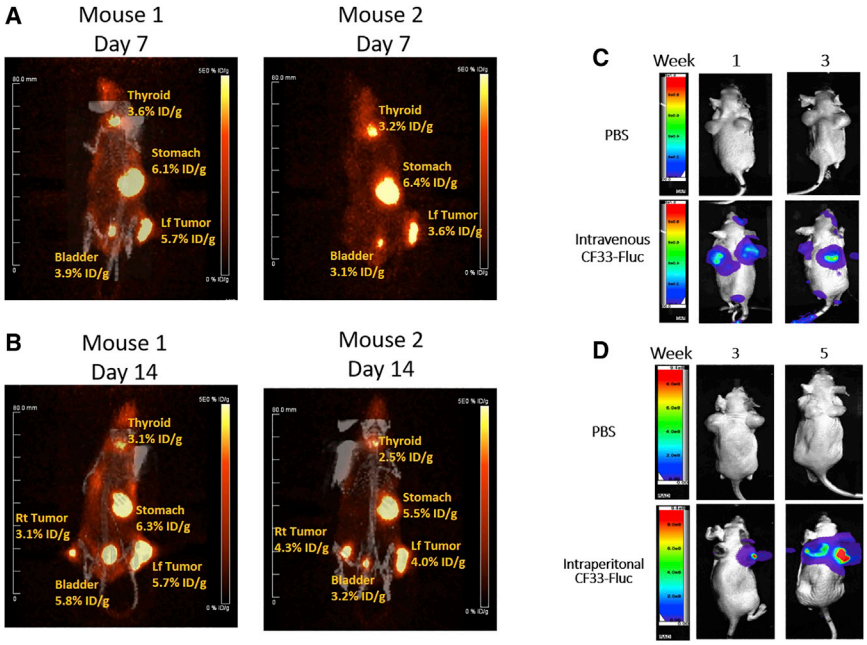

Figure 1. PET imaging of ^{124}I uptake and bioluminescent luciferase shows CF33-hNIS and CF33-Fluc tumor tropism

Mice bearing bilateral HT29 flank xenografts were injected in the left flank tumor with CF33-hNIS. (A) On day 7 following viral injection, robust uptake is noted in the injected left-side tumor. (B) On day 14, tumor tropism is shown via uptake in the non-injected right-side tumor. Mice bearing bilateral HCT116 flank xenografts were injected i.v. or i.p. with CF33-Fluc. (C and D) Both i.v. (C) and i.p. (D) delivery of CF33-Fluc resulted in tumor luminescence.

induced anti-tumor immune responses also remains elusive. *In vivo* and *ex vivo* techniques for radiolabeling immune cells, cytokines, and co-stimulators or co-inhibitors are rapidly evolving arenas of clinical imaging. To most comprehensively understand the anti-tumor effects of viroimmunotherapy without invasively sampling tissue, non-invasive imaging should include viral tracking, measurement of immune checkpoint expression, and tracking immune cells into tumors. Herein, we review progress and promise of comprehensive non-invasive imaging of viroimmunotherapy.

REVIEW OF PUBLISHED CLINICAL REAL-TIME VIRAL TRACKING

As demonstrated by our group and others, real-time tracking of viral replication demonstrates tumor tropism whether viruses are administered intratumorally (i.t.), intravenously (i.v.), or intraperitoneally (i.p.) (Figure 1).[16,17] These experiments were confirmed in previously published experiments using HCT116 xenografts,[17] and also as shown here using HT-29 xenografts infected with a recombinant orthopoxvirus platform (CF33) with *tk* deletion encoding either hNIS (CF33-hNIS) or firefly luciferase (Fluc) (CF33-Luc).[16,17]

Upon comprehensive English literature review from 1995 to present, many abstracts and posters referencing images on replicating OVs were found. However, a surprising paucity of peer-reviewed publications showed images of non-invasive viral replication tracking. We were only able to identify six peer-reviewed publications with images of viral replication: four studies demonstrated successful tracking of NIS-encoding OVs via I-123 SPECT/CT, one study used an ^{18}F-labeled penciclovir analog, and one study used a ^{124}I-labeled substrate for herpes simplex virus 1 (HSV-1)-*tk* to monitor thymidine kinase gene expression (Table 1). In each of the described studies, the success of imaging appeared to be dose-dependent. In the NIS-based studies, images appeared most consistently 7–8 days after treatment.[10–12] In the *tk* imaging papers, Jacobs et al.[15] show [^{124}I]-FIAU retention 68 h after injection, whereas Peñuelas et al.[14] examined the [^{18}F]-FHBG signal 1 week after injection.[14,15] In the remaining trial referenced in Table 1, investigators of a GFP-encoding vaccinia used fluorescent lamps in the clinic to examine a pox-like rash occurring in treated patients with head and neck carcinomas. While this does not represent imaging of viral replication in tumors, the investigators emphasize that such a rash confirms successful systemic viral replication.[8]

Clinical OV image optimization has remained a challenge despite numerous creative adjuncts such as oral contrast,[18] chemo-tagged radiotracers, and novel highly specific tracers.[19] Moreover, in addition to the expected variability of viral replication between tumor types, even similar types of tumors in identical anatomic locations exhibit show differences in viral replication. For instance, Rajecki et al.[20] treated a cervical cancer patient with Ad5/3-Δ24-hNIS, acting based upon the findings of Barton et al.[13] using Ad5-yCD/*mut*TK$_{SR39}$*rep*-hNIS in prostate cancer. Unfortunately, Rajecki et al. saw no evidence of an OV-based signal. This may have been due to their study of both a different vector with hNIS on a different promoter, and also an entirely different disease type. Groups using hNIS-based imaging have seen more consistent results at higher doses and with more uniform disease states as detailed in Table 1. However, published images demonstrate that further optimization is needed to achieve clinical relevance. Perhaps clinical optimization using more potent and rapidly replicating virus platforms such as CF33 or HSVs encoding hNIS will render consistent high-yield imaging to guide future therapies. If properly established, real-time non-invasive deep tissue imaging will enable more rapid incorporation of imageable viroimmunotherapies into solid tumor treatment schema.

VIRAL REPLICATION CO-LOCALIZES WITH TUMOR T CELL INFILTRATION

To further assess whether non-invasive viral imaging can serve as a linear surrogate for both viral replication and T cell infiltration, we

Table 1. Studies that include imaging for tracking virus

Year, journal, authors	Virus	Dose (route)	No. of images per no. of patients in trial	Disease treated	Actual image	Trial ID
2001, Lancet, Jacobs et al.[15]	HSV-1-*tk* in liposomal vector DAC-30	unclear PFU in 30 mL (i.t.)	1/5	recurrent glioblastoma	[^{124}I]-FIAU-PET MET-PET FDG-PET MRI brain	none listed
2005, Gastroenterology, Peñuelas et al.[14]	AdCMVtk	2e10–2e12 (i.t.)	4/7 high dose only	hepatocellular carcinoma	PET-CT MRI [^{18}F]FHBG-PET torso	none listed
2008, Molecular Therapy, Barton et al.[13]	Ad5-yCD*ut*TK$_{SR39}$*rep*-hNIS	1e11–1e12 (intraprostatic)	7/12	prostate cancer	SPECT/CT of pelvis of multiple patients	ClinicalTrials.gov: NCT00583492
2014, Mayo Clinic Proceedings, Russell et al.[12]	MV-NIS	1e6–1e11 (i.v.)	2/2	recurrent plasma cell myeloma	PET/CT of forehead, SPECT/CT and PET of whole body on days 1, 8, 15, and 28	ClinicalTrials.gov: NCT00450814
2015, Cancer Research, Galanis et al.[11]	MV-NIS	1e8–1e9 (i.p.)	3/16 high dose only	drug-resistant ovarian cancer	SPECT/CT left pelvis tumor	ClinicalTrials.gov: NCT00408590
2017, Clinical Cancer Research, Mell et al.[8]	GL-ONC1	3e8–3e9 (i.v.)	no. images not reported/19	locoregionally advanced head and neck carcinoma	fluorescent image of pox lesions noting systemic infection	ClinicalTrials.gov: NCT01584284
2017, Leukemia, Dispenzieri et al.[10]	MV-NIS	1e6–1e11 (i.v.)	8/32	refractory multiple myeloma	SPECT/CT of legs with light-up on day 7 post-treatment	NCT 00450814

confirmed that immunofluorescent vaccinia staining corresponds to immunohistochemical (IHC) staining showing T cells co-localizing with viral infection (Figures 2A and 2B). Moreover, in subsequent experiments, we evaluated immune cell infiltration and confirmed these IHC findings quantitatively using flow-cytometry on single cells obtained from tumors to find that CD8$^+$ tumor infiltration is higher in viral-treated tumors (Figure 2C). We and others have shown that CD8$^+$ T cells co-localize to actively replicating virus.[21] This is aligned with findings by Sampath et al.[22] that showed direct synergistic interactions between an enveloped vaccinia virus and immune cell components. While co-localized viral particles and immune cells suggest that non-invasive imaging of viral replication corresponds to immune cell trafficking, only by specifically imaging immune cells or invasively sampling tumors can we confirm this.

IMAGING VIRALLY INDUCED IMMUNE CHECKPOINT EXPRESSION

Our group and others have demonstrated upregulated PD-L1 in tumors following poxvirus infection.[21,23] Many think that such upregulation mediates the success of combination therapies pairing OVs with checkpoint inhibitors in advanced solid tumors.[24] Others think that viruses pair well with checkpoint inhibitors simply because they release inflammatory damage- and pathogen-associated proteins into the tumor microenvironment, thereby recruiting and activating immune cells in the tumor microenvironment.[25] In order to find the most effective place in treatment algorithms for OVs amid the already tumultuous sea of immune checkpoint inhibitors available, we must fully characterize both checkpoint expression and immune cell trafficking in real time. While reliably imaging checkpoint expression after immunotherapy treatment of any sort is a tall order, there is some progress with radiolabeled antibodies to a variety of checkpoint proteins (Figure 3). Indeed, one can image any point along the continuum of activating a T cell as it recognizes tumor, from radio-labeled antibodies to cytokines such as interferon (IFN)γ, cluster of differentiation (CD) cell-surface proteins such as CD8, or markers of activation such as granzyme B. At present, *in vivo* imaging of this nature is plagued by non-specific background uptake. That said, some progress is being made with highly specific radiotracers and antibodies.[26]

CURRENT CLINICAL PROGRESS IN TRACKING IMMUNE RESPONSES TO OV

To date, imaging of immune responses to viral therapy are sparsely explored. In 2013, Weibel et al.[27] correlated ^{19}F-magnetic resonance imaging (MRI) with CD68 staining on IHC in xenograft models of human melanoma and breast cancer infected with an oncolytic vaccinia virus GLV-1h68. These macrophage-dense regions within a tumor tended to surround virally infected areas of tumor as confirmed with immunofluorescence staining. While this suggests that ^{19}F-MRI could serve as a surrogate for tracking immune response to treatment, clinical translatability of these findings in nude mice is questionable. To take the next steps as a field in imaging immune responses to oncolytic viral therapy, we will need to draw from the experiences of our adoptive immune cell colleagues.

Ex vivo radiolabeling of T cells holds promise to help track efficacy of immunotherapies (Figure 4) in terms of immune cell recruitment.[28] While this is most broadly explored to track T cells bearing radiolabeled chimeric antigen receptors (CARs), simple co-culture of T cells with radioisotope is also an effective means of tracking tumor infiltration. Perhaps the most clinically advanced form of *in vivo* targeting and also adoptive cell radiolabeling is found in zirconium (89-Zr).[29] Notably more specific than other tracers such as 18-F given its independence from glucose metabolism,[30] 89-Zr also has the advantages of a long half-life (3.3 days), making it helpful for tracking

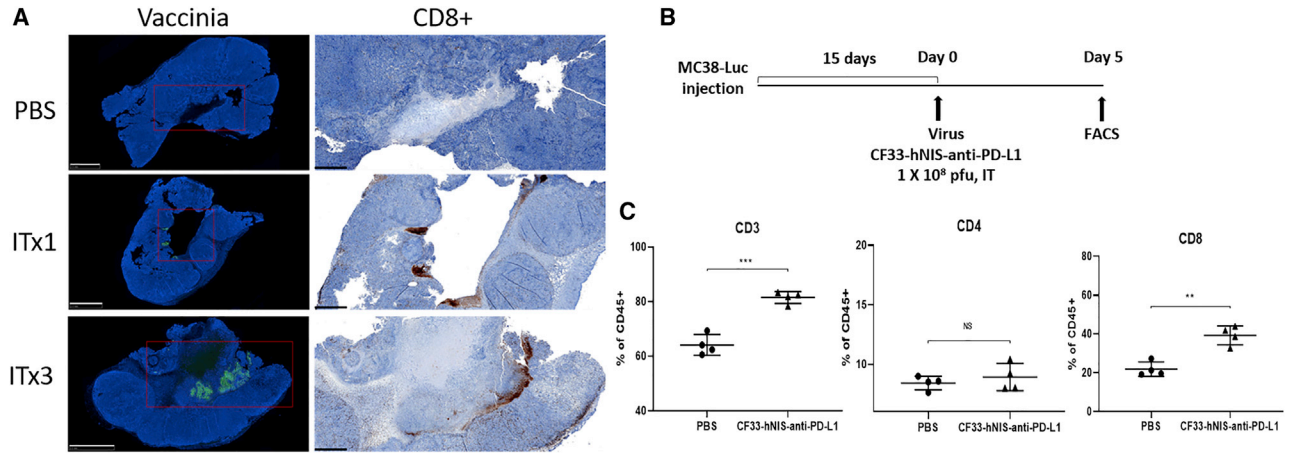

Figure 2. Virus co-localizes with tumor-infiltrating T cells

(A) On day 10 after intra-tumoral injection of CF33-Fluc, immunofluorescence vaccinia staining and immunohistochemical CD8$^+$ T cell staining shows co-localization of virally infected cells and tumor-infiltrating T cells. Vaccinia average original magnification, ×0.8; scale bars, 5 mm. CD8$^+$ original magnification, ×2; scale bars, 1 mm. (B) Treatment schema. (C) Confirmatory experiments using flow cytometry of tumor lysates showed increased CD8$^+$ T cell infiltration as early as 5 days following viral injection. n = 4/group. $^{**}p < 0.01$, $^{***}p < 0.001$, by unpaired t test with Welch's correction.

cells during at least several days with serial CT-PET imaging.[29] Moreover, its relatively lower positron energy fosters enhanced resolution of PET images. While other more specific tracers such as copper are also being studied, the half-life is comparatively short and the background signal is also prohibitive in some cases. ^{89}Zr-labeled T cells have been successfully used in clinical settings to image CAR-T cell trafficking to non-small cell lung cancer (NSCLC), prostate cancer, melanoma, and advanced gastrointestinal malignancies as detailed in Table 2.[26,31–33] While the alternative of MRI uses superparamagnetic iron oxide nanoparticles that are ingested by cells intended for tracking, this is a much more cumbersome and lengthy image acquisition process that is also highly dependent on cell function rather than precise labeling, as would be required for comprehensive imaging of viroimmunotherapy.

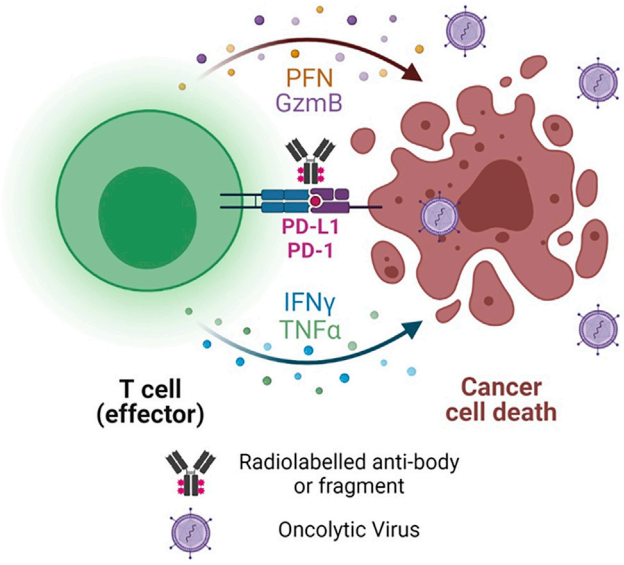

Figure 3. *In vivo* labeling of virally induced immune checkpoint upregulation

The authors propose that an ideal strategy toward comprehensively imaging responses to oncolytic viroimmunotherapy would take into account the "big picture" of a tumor transformation following viral infection, including (1) immediate changes to cancer cells upon viral entry and replication, (2) initial changes to the surrounding tumor immune microenvironment, and (3) alterations in tumor immune cell infiltration (Figure 5A). Each of these three components of virally mediated tumor transformation is imageable by tracking virus to tumor with reporter genes, then flagging upregulation of immune checkpoints, and monitoring effector immune cell traffic in treated tumors (Figure 5B). In so doing, investigators would be able to amend treatment courses in real time to optimize anti-tumor immune responses and prolong patient survival.

CONCLUSIONS

Herein, we have reviewed the published clinical experience with functional viral imaging and proposed additional possible future directions for tracking viral replication in clinical studies. We further reviewed current progress and challenges as well as strategies for future comprehensive imaging of immune responses to oncolytic viral treatment. In conclusion, this paper emphasizes the importance of continued optimization of preclinical and clinical protocols to visualize viral replication in real time. While many trials are currently testing imaging endpoints, we must encourage further investigations to both speed regulatory approvals and incorporate viroimmunotherapy into treatment algorithms. In this era of pay-to-play immunotherapy, patients, clinicians, and payers alike should place a high value

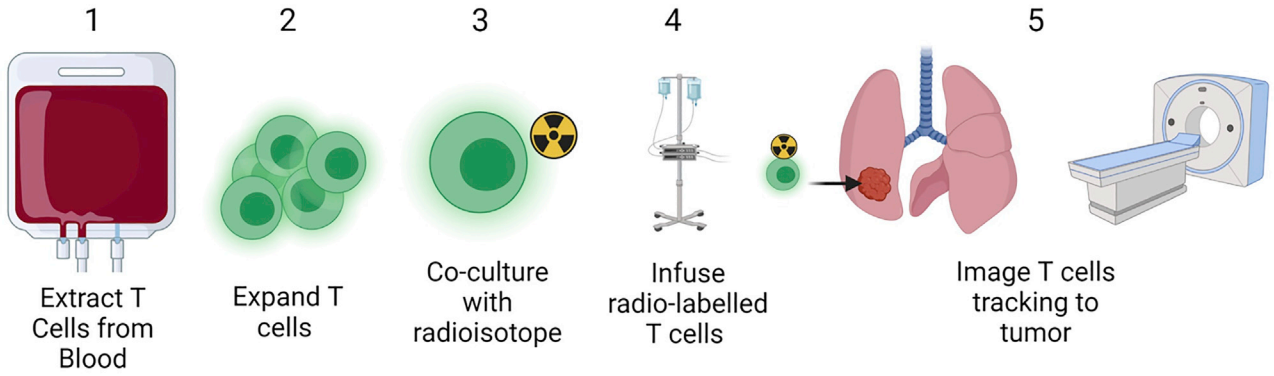

Figure 4. *Ex vivo* radiolabeling T cells and imaging to track those cells *in vivo*

on real-time proof of viral tumor tropism and therapeutic benefit. Strategies to non-invasively and reliably image viral delivery, checkpoint expression, and immune cell trafficking will be critical to advancement of the field.

LITERATURE REVIEW

PubMed and ClinicalTrials.gov were queried for search terms including, but not limited to, oncolytic virus, SPECT, PET, imaging, NIS, GFP, optical imaging, functional imaging, and tracking. All active clinical trials involving oncolytic viral imaging were reviewed. Trial vectors and key words were used in PubMed to search for any publications of results. Many trials are still accruing data.[9,34] Identified publications were included in Table 1 only when a clinically generated image was a figure in the manuscript. There were many published abstracts without images available, and we anticipate that images will be forthcoming from several groups in the near future.

VIRUS CHIMERIZATION AND hNIS OR FLUC CLONING

The chimerization, cloning, competitive selection, and sequence of CF33 backbone virus have been described previously.[35–38] Insertion of the hNIS expression cassette or Fluc under the control of the vaccinia H5 promoter or synthetic early (SE) promoter at the *J2R* locus has also been described,[16,17] as has the deletion of the *F14.5L* gene[36] and insertion of the anti-PD-L1 transgene at the *F14.5L* locus.[39]

In vitro luciferase activity was confirmed by infecting HCT-116 cells with CF33-Fluc at varying multiplicities of infection (MOIs). Rapid luciferase activity was observed after 24 h by adding 100× luciferin solution (prepared as below) directly to wells and imaging after 10 min with a Lago X optical imaging system (Spectral Instruments Imaging, Tucson, AZ, USA).

CELL LINES

HT-29 (RRID:CVCL_0320), HCT116 (RRID:CVCL_0291), and African green monkey kidney fibroblasts-CV-1 (RRID:CVCL_0229) cell lines were purchased from ATCC (Manassas, VA, USA). All human colorectal cell lines were maintained in McCoy's 5A medium (Gibco, Gaithersburg, MD, USA) and CV-1 cells were maintained in Dulbecco's modified Eagle's medium (Corning Life Sciences, Corning, NY, USA). MC38 and MC38-Luc cells were a kind gift from Dr. Laleh Melstrom's laboratory (City of Hope, Duarte, CA, USA). MC38 and MC38-Luc cells were maintained in DMEM. All cells were supplemented with 10% fetal bovine serum (FBS) and 1% antibiotic-antimycotic solution, both purchased from Corning Life Sciences

Table 2. Zirconium-89 based imaging to track therapeutics

Year, Journal, Author	Image modality	What labeled	No. of patients imaged	Disease process	Trial ID
2016, Journal of Nuclear Medicine, Pandit-Taskar et al.[31]	PET and SPECT	^{89}Zr-Df-IAB2M	18	prostate Cancer	ClinicalTrials.gov: NCT02760199
2017, Nature Communications, Niemeijer et al.[32]	PET-CT	^{89}Zr-nivolumab	13	NSCLC	2015-004760-11 (EU)
2018, J Clinical Oncology, Postow et al.[26]	PET-CT	^{89}Zr-IAB22M2C (anti-CD8)	3	melanoma, HCC, NSCLC	ClinicalTrials.gov: NCT03107663
2019, Clinical Cancer Research, Moek et al.[33]	PET-CT	^{89}Zr-AMG211 (BiTE CEA/CD3)	9	advanced GI cancer	ClinicalTrials.gov: NCT02291614
ClinicalTrials.gov	PET-CT	^{89}Zr-Df -IAB22M2C (anti-CD8)	ongoing	melanoma, NSCLC, RCC, SCC	ClinicalTrials.gov: NCT03802123

HCC, hepatocellular carcinoma; GI, gastrointestinal; RCC, renal cell carcinoma; SCC, squamous cell carcinoma.

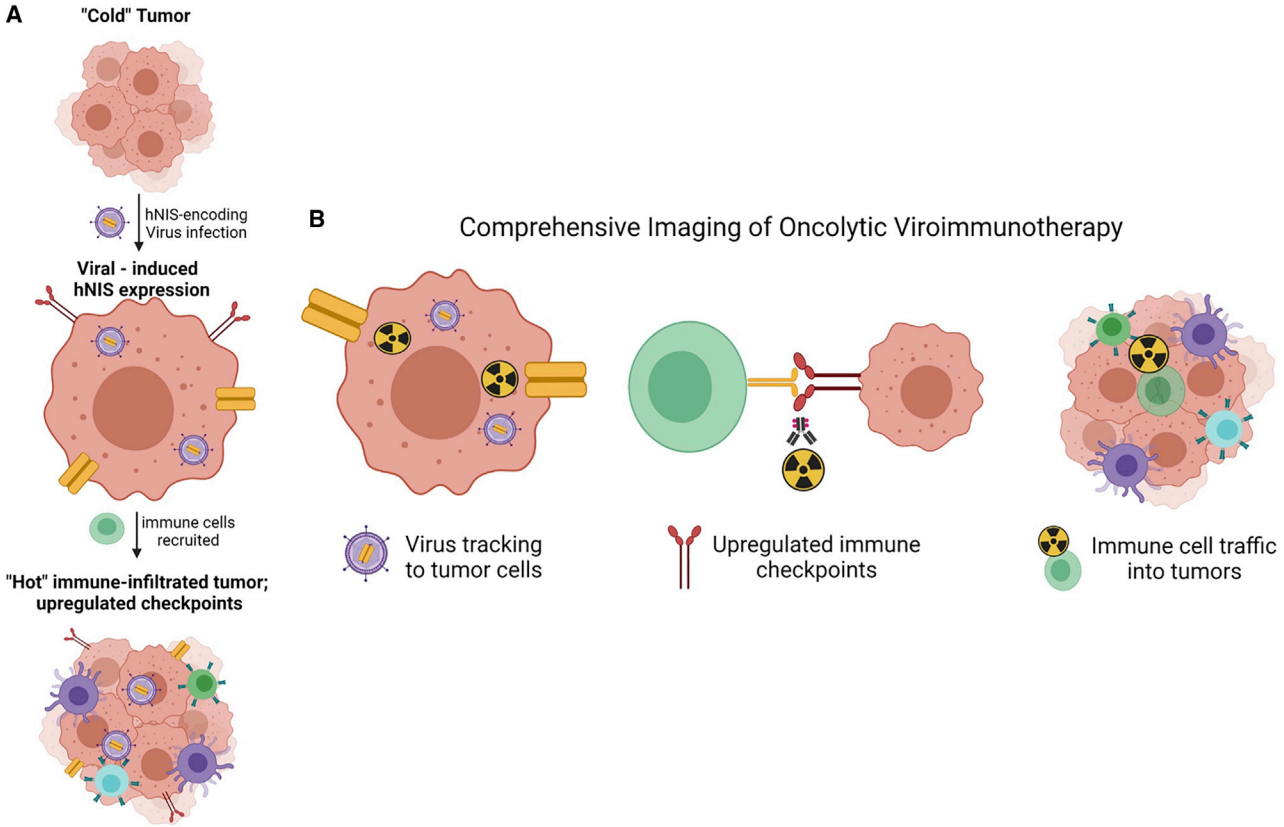

Figure 5. Virus-induced tumor changes strategies for comprehensive imaging

(A) Schematic showing a "cold" tumor devoid of effector immune cells infected with oncolytic virus, expressing functional reporter protein such as hNIS, upregulating immune checkpoint expression, and recruiting and activating immune cells. (B) Opportunities for radiolabeling each step of viral immunogenicity from hNIS expression, resulting in radioisotope uptake to antibody tagging of immune checkpoints to infusing radiolabeled immune cells and examining their trafficking to tumors.

(Corning, NY, USA). The cells were maintained in a humidified incubator at 37°C and 5% CO_2. Efforts were made not to perform experiments past 15 passages of cells. All cell lines were tested for mycoplasma before each experiment initiation.

PET IMAGING

In vivo I-124 uptake measured by PET/CT

Mice bearing HT-29 flank xenografts were divided into imaging and control groups (n = 4 mice). To analyze tumor imageability after intratumoral delivery, mice received an intratumoral injection of 10^4 plaque-forming units (PFU) per tumor of either CF33-hNIS, CF33-Fluc, or PBS when tumors reached 100 mm^3. At 7, 14, and 21 days after viral injection, mice in each group received 200 μCi of I-124 injected per tail vein. The radioisotope was obtained from the City of Hope Small Animal Imaging Core Radiopharmacy. PET imaging was then obtained 2 h following injection using the small animal PET scanner (microPET R4, Siemens), which provides fully three-dimensional PET imaging with a spatial resolution of better than 2.0 mm and quantitative accuracy for measurement of tissue activity concentration on the order of 10%. Quantitative accuracy is supported by scatter, dead time, and measured attenuation corrections. The system includes a fully developed image analysis package that supports volumetric regions of interest and the fusion of PET with co-registered anatomic CT. To protect mouse thyroids from radioiodine ablation, all mice received T4 supplementation with 5 mg of levothyroxine/L of water beginning 1 week before radioiodine administration.

LUCIFERASE IMAGING

Firefly luciferin solution was prepared as per the manufacturer's instruction (PerkinElmer, Waltham, MA, USA). Imaging was obtained after intraperitoneal delivery of luciferin in a control mouse and all mice treated with CF33-Fluc using a Lago X optical imaging system (Spectral Instruments Imaging, Tucson, AZ, USA) after 15 minutes of incubation.

TUMOR MODELS AND VIRUS DOSING

For the HCT116 xenograft model, 2–3 × 10^6 of HTCT116 cells were injected into 6- to 8-week-old female nude mouse flank using a total of 100 μL of PBS containing 50% Matrigel for each tumor. When the average tumor size approached 150 mm^3, mice were divided into experimental groups and treated with 10^5 PFU of CF33-Fluc in 50 μL of PBS by intravenous or intraperitoneal injection.

Flank tumors of MC38 and MC38-Luc were established using 3–5 × 10^5 cells in Matrigel. Tumor measurements and mouse weight were monitored twice weekly using calipers to calculate tumor volume, V (mm^3) = (0.5) × A^2 x B, where A is the shortest measurement and B is the longest measurement. Treatment typically occurred when tumors reached 100–200 mm^3 (approximately 10 days after cell injection), following which mice were randomized into treatment groups (n = 4) such that average tumor volume in each group was similar. C57BL/6J mice 8–12 weeks of age were used for most experiments (Jackson Laboratory, Bar Harbor, ME, USA and Charles River Laboratories, Wilmington, MA, USA, RRID:IMSR_JAX:000664, RRID:IMSR_CRL:027). Six-week-old Hsd:athymic nude-Foxn1nu female mice (Envigo, Indianapolis, IN, USA) were purchased and acclimatized for 7 days.

Mice were maintained in a biosafety containment level 2 facility within our vivarium where the environment was temperature and light controlled with 12-h light/12-h dark cycles, and food and water were ingested *ad libitum*. All animal experiments were performed with approval of the City of Hope Institutional Animal Care and Use Committee (IACUC).

IHC

Tumors were harvested and fixed with 10% formalin. Paraffin-embedded 5-μm-thick tumor sections were obtained. The slides were deparaffinized followed by heat-mediated antigen retrieval per the manufacturer's protocol (IHC World, Ellicott City, MD, USA). Tumor slides were then permeabilized with cold methanol and blocked for 30 min with TNB blocking buffer (PerkinElmer, Waltham, MA, USA). Tumor slides were incubated with a rabbit anti-vaccinia virus antibody (Abcam, Cambridge, MA, USA, RRID:AB_778768) 1:100 in TNB blocking buffer in a humidified chamber at 4°C overnight. The next day, tumor slides were stained with Alexa Fluor 488-conjugated goat anti-rabbit (Abcam, Cambridge, MA, USA, RRID:AB_2630356) 1:200 in TNB blocking buffer for 1 h at room temperature. Finally, the slides were counterstained with 4′,6-diamidino-2-phenylindole (DAPI). IHC for CD8 was performed by the Pathology Core at City of Hope. Images were obtained using the Nanozoomer 2.0HT digital slide scanner (Hamamatsu Photonics, Hamamatsu, Japan) or Ventana iScan HT (Roche, Basel, Switzerland).

FLOW CYTOMETRY

Single cells from tumors were generated using mouse a tumor dissociation kit utilizing a gentleMACS dissociator (Miltenyi Biotec, Cologne, Germany). Cells were stained with Live/Dead Fixable dye (Invitrogen, Carlsbad, CA, USA) in PBS for 30 min at 4°C in the dark. Next, Fc receptors on the cells were blocked using an anti-CD16/32 antibody (BD Biosciences, Franklin Lakes, NJ, USA, RRID:AB_394657 in FACS buffer (PBS containing 2% FBS) for 10 min and then stained for 30 min at 4°C in the dark using the following antibodies: mouse CD45-peridinin chlorophyll protein complex (PerCP) (BioLegend, San Diego, CA, USA, RRID:AB_893340), mouse CD3-fluorescein isothiocyanate (FITC) (eBiosciences, San Diego, CA, USA RRID:AB_2572431), mouse CD4-allophycocyanin (APC) (BioLegend, San Diego, CA, USA, RRID:AB_389325), and mouse CD8- VioGreen (Miltenyi Biotec, Cologne, Germany, RRID:AB_2659495). The data were acquired using the MACSQuant analyzer 10 (Miltenyi Biotec, Cologne, Germany). Data were analyzed using FlowJo software (v10, Tree Star, Ashland, OR, USA).

STATISTICAL ANALYSIS

Statistical analysis was performed using GraphPad Prism (version 7.01, GraphPad, La Jolla, CA, USA). A Student's t test was used to evaluate statistical significance. $p < 0.05$ was considered significant. Where present in figures, error bars indicate SD or SEM as defined in legends.

ACKNOWLEDGMENTS

This work was supported by the American Cancer Society Mentored Research Scholar Grant MRSG-16-047-01-MPC. S.C. and S.G.W. were supported by the generosity of the Natalie and David Roberts Family. The authors wish to acknowledge Dr. Supriya Deshpande for expert editorial assistance. This work was completed using the Beckman Research Institute shared facilities that are supported in part by the National Cancer Institute of the National Institutes of Health Grant P30CA033572. Figures were created using BioRender. S.C. is supported by California Breast Cancer Research Program (Award B261B1393)

AUTHOR CONTRIBUTIONS

Study concept and design, S.C., S.-I.K., M.O., Y.F., Y.W., and A.K.P.; data collection, analysis, and interpretation, S.C., S.-I.K., M.O., J.L., S.K., Z.Z., A.Y., Y.F., and S.G.W.; manuscript preparation and critical revision, all authors; and final approval of manuscript, all authors.

DECLARATION OF INTERESTS

Y.F. receives royalties from Merck and from Imugene. CF33 platform is licensed to Imugene by the City of Hope. The remaining authors are City of Hope employees.

REFERENCES

1. Andtbacka, R.H., Agarwala, S.S., Ollila, D.W., Hallmeyer, S., Milhem, M., Amatruda, T., Nemunaitis, J.J., Harrington, K.J., Chen, L., Shilkrut, M., et al. (2016). Cutaneous head and neck melanoma in OPTiM, a randomized phase 3 trial of talimogene laherparepvec versus granulocyte-macrophage colony-stimulating factor for the treatment of unresected stage IIIB/IIIC/IV melanoma. Head Neck *38*, 1752–1758.
2. Andtbacka, R.H., Kaufman, H.L., Collichio, F., Amatruda, T., Senzer, N., Chesney, J., Delman, K.A., Spitler, L.E., Puzanov, I., Agarwala, S.S., et al. (2015). Talimogene laherparepvec improves durable response rate in patients with advanced melanoma. J. Clin. Oncol. *33*, 2780–2788.
3. Andtbacka, R.H., Ross, M., Puzanov, I., Milhem, M., Collichio, F., Delman, K.A., Amatruda, T., Zager, J.S., Cranmer, L., Hsueh, E., et al. (2016). Patterns of clinical response with talimogene laherparepvec (T-VEC) in patients with melanoma treated in the OPTiM phase III clinical trial. Ann. Surg. Oncol. *23*, 4169–4177.
4. Harrington, K.J., Andtbacka, R.H., Collichio, F., Downey, G., Chen, L., Szabo, Z., and Kaufman, H.L. (2016). Efficacy and safety of talimogene laherparepvec versus granulocyte-macrophage colony-stimulating factor in patients with stage IIIB/C and IVM1a melanoma: Subanalysis of the phase III OPTiM trial. OncoTargets Ther. *9*, 7081–7093.
5. Ma, Y., Wang, Q., Dong, Q., Zhan, L., and Zhang, J. (2019). How to differentiate pseudoprogression from true progression in cancer patients treated with immunotherapy. Am. J. Cancer Res. *9*, 1546–1553.

6. Serganova, I., and Blasberg, R.G. (2019). Molecular imaging with reporter genes: Has its promise been delivered? J. Nucl. Med. *60*, 1665–1681.

7. Zheng, M., Huang, J., Tong, A., and Yang, H. (2019). Oncolytic viruses for cancer therapy: Barriers and recent advances. Mol. Ther. Oncolytics *15*, 234–247.

8. Mell, L.K., Brumund, K.T., Daniels, G.A., Advani, S.J., Zakeri, K., Wright, M.E., Onyeama, S.J., Weisman, R.A., Sanghvi, P.R., Martin, P.J., et al. (2017). Phase I trial of intravenous oncolytic vaccinia virus (GL-ONC1) with cisplatin and radiotherapy in patients with locoregionally advanced head and neck carcinoma. Clin. Cancer Res. *23*, 5696–5702.

9. Wu, Z.J., Tang, F.R., Ma, Z.W., Peng, X.C., Xiang, Y., Zhang, Y., Kang, J., Ji, J., Liu, X.Q., Wang, X.W., et al. (2018). Oncolytic viruses for tumor precision imaging and radiotherapy. Hum. Gene Ther. *29*, 204–222.

10. Dispenzieri, A., Tong, C., LaPlant, B., Lacy, M.Q., Laumann, K., Dingli, D., Zhou, Y., Federspiel, M.J., Gertz, M.A., Hayman, S., et al. (2017). Phase I trial of systemic administration of Edmonston strain of measles virus genetically engineered to express the sodium iodide symporter in patients with recurrent or refractory multiple myeloma. Leukemia *31*, 2791–2798.

11. Galanis, E., Atherton, P.J., Maurer, M.J., Knutson, K.L., Dowdy, S.C., Cliby, W.A., Haluska, P., Jr., Long, H.J., Oberg, A., Aderca, I., et al. (2015). Oncolytic measles virus expressing the sodium iodide symporter to treat drug-resistant ovarian cancer. Cancer Res. *75*, 22–30.

12. Russell, S.J., Federspiel, M.J., Peng, K.W., Tong, C., Dingli, D., Morice, W.G., Lowe, V., O'Connor, M.K., Kyle, R.A., Leung, N., et al. (2014). Remission of disseminated cancer after systemic oncolytic virotherapy. Mayo Clin. Proc. *89*, 926–933.

13. Barton, K.N., Stricker, H., Brown, S.L., Elshaikh, M., Aref, I., Lu, M., Pegg, J., Zhang, Y., Karvelis, K.C., Siddiqui, F., et al. (2008). Phase I study of noninvasive imaging of adenovirus-mediated gene expression in the human prostate. Mol. Ther. *16*, 1761–1769.

14. Peñuelas, I., Mazzolini, G., Boán, J.F., Sangro, B., Martí-Climent, J., Ruiz, M., Ruiz, J., Satyamurthy, N., Qian, C., Barrio, J.R., et al. (2005). Positron emission tomography imaging of adenoviral-mediated transgene expression in liver cancer patients. Gastroenterology *128*, 1787–1795.

15. Jacobs, A., Voges, J., Reszka, R., Lercher, M., Gossmann, A., Kracht, L., Kaestle, C., Wagner, R., Wienhard, K., and Heiss, W.D. (2001). Positron-emission tomography of vector-mediated gene expression in gene therapy for gliomas. Lancet *358*, 727–729.

16. O'Leary, M.P., Warner, S.G., Kim, S.I., Chaurasiya, S., Lu, J., Choi, A.H., Park, A.K., Woo, Y., Fong, Y., and Chen, N.G. (2018). A novel oncolytic chimeric orthopoxvirus encoding luciferase enables real-time view of colorectal cancer cell infection. Mol. Ther. Oncolytics *9*, 13–21.

17. Warner, S.G., Kim, S.I., Chaurasiya, S., O'Leary, M.P., Lu, J., Sivanandam, V., Woo, Y., Chen, N.G., and Fong, Y. (2019). A novel chimeric poxvirus encoding hNIS is tumor-tropic, imageable, and synergistic with radioiodine to sustain colon cancer regression. Mol. Ther. Oncolytics *13*, 82–92.

18. Suksanpaisan, L., Pham, L., McIvor, S., Russell, S.J., and Peng, K.W. (2013). Oral contrast enhances the resolution of in-life NIS reporter gene imaging. Cancer Gene Ther. *20*, 638–641.

19. Jiang, H., and DeGrado, T.R. (2018). [^{18}F]tetrafluoroborate ([^{18}F]TFB) and its analogs for PET imaging of the sodium/iodide symporter. Theranostics *8*, 3918–3931.

20. Rajecki, M., Kangasmaki, A., Laasonen, L., Escutenaire, S., Hakkarainen, T., Haukka, J., Ristimaki, A., Kairemo, K., Kangasniemi, L., Kiljunen, T., et al. (2011). Sodium iodide symporter SPECT imaging of a patient treated with oncolytic adenovirus Ad5/3-Δ24-hNIS. Mol. Ther. *19*, 629–631.

21. Kim, S., Park, A.K., Chaurasiya, S., Kang, S., Lu, J., Yang, A., Sivanandam, V., Zhang, Z., Woo, Y., Priceman, S.J., et al. (2021). Recombinant orthopoxvirus primes colon cancer for checkpoint inhibitor and cross-primes T cells for anti-tumor and anti-viral immunity. Mol. Cancer Ther. *20*, 173–182.

22. Sampath, P., Li, J., Hou, W., Chen, H., Bartlett, D.L., and Thorne, S.H. (2013). Crosstalk between immune cell and oncolytic vaccinia therapy enhances tumor trafficking and antitumor effects. Mol. Ther. *21*, 620–628.

23. Liu, Z., Ravindranathan, R., Kalinski, P., Guo, Z.S., and Bartlett, D.L. (2017). Rational combination of oncolytic vaccinia virus and PD-L1 blockade works synergistically to enhance therapeutic efficacy. Nat. Commun. *8*, 14754.

24. Ribas, A., Dummer, R., Puzanov, I., VanderWalde, A., Andtbacka, R.H.I., Michielin, O., Olszanski, A.J., Malvehy, J., Cebon, J., Fernandez, E., et al. (2017). Oncolytic virotherapy promotes intratumoral t cell infiltration and improves anti-PD-1 immunotherapy. Cell *170*, 1109–1119.e10.

25. Gujar, S., Pol, J.G., and Kroemer, G. (2018). Heating it up: Oncolytic viruses make tumors 'hot' and suitable for checkpoint blockade immunotherapies. OncoImmunology *7*, e1442169.

26. Postow, M.A., Harding, J.J., Hellmann, M.D., Gordon, M.S., Tsai, F., Donoghue, J.A.O., Lewis, J.S., Wu, A.M., Le, W., Korn, R.L., et al. (2018). Imaging of tumor infiltrating T cells with an anti-CD8 minibody (Mb) 89Zr-IAB22M2C, in advanced solid tumors *36* (15 Suppl), e24160.

27. Weibel, S., Basse-Luesebrink, T.C., Hess, M., Hofmann, E., Seubert, C., Langbein-Laugwitz, J., Gentschev, I., Sturm, V.J.F., Ye, Y.X., Kampf, T., et al. (2013). Imaging of intratumoral inflammation during oncolytic virotherapy of tumors by F-19-magnetic resonance imaging (MRI). PLoS ONE *8*, e56317.

28. McCarthy, C.E., White, J.M., Viola, N.T., and Gibson, H.M. (2020). *In vivo* imaging technologies to monitor the immune system. Front. Immunol. *11*, 1067.

29. Kurebayashi, Y., Choyke, P.L., and Sato, N. (2021). Imaging of cell-based therapy using ^{89}Zr-oxine *ex vivo* cell labeling for positron emission tomography. Nanotheranostics *5*, 27–35.

30. Stojanov, K., de Vries, E.F., Hoekstra, D., van Waarde, A., Dierckx, R.A., and Zuhorn, I.S. (2012). [^{18}F]FDG labeling of neural stem cells for in vivo cell tracking with positron emission tomography: Inhibition of tracer release by phloretin. Mol. Imaging *11*, 1–12.

31. Pandit-Taskar, N., O'Donoghue, J.A., Ruan, S., Lyashchenko, S.K., Carrasquillo, J.A., Heller, G., Martinez, D.F., Cheal, S.M., Lewis, J.S., Fleisher, M., et al. (2016). First-in-human imaging with 89Zr-Df-IAB2M anti-psma minibody in patients with metastatic prostate cancer: Pharmacokinetics, biodistribution, dosimetry, and lesion uptake. J. Nucl. Med. *57*, 1858–1864.

32. Niemeijer, A.N., Leung, D., Huisman, M.C., Bahce, I., Hoekstra, O.S., van Dongen, G.A.M.S., Boellaard, R., Du, S., Hayes, W., Smith, R., et al. (2018). Whole body PD-1 and PD-L1 positron emission tomography in patients with non-small-cell lung cancer. Nat. Commun. *9*, 4664.

33. Moek, K.L., Waaijer, S.J.H., Kok, I.C., Suurs, F.V., Brouwers, A.H., Menke-van der Houven van Oordt, C.W., Wind, T.T., Gietema, J.A., Schröder, C.P., Mahesh, S.V.K., et al. (2019). ^{89}Zr-labeled bispecific T-cell engager AMG 211 PET shows AMG 211 accumulation in CD3-rich tissues and clear, heterogeneous tumor uptake. Clin. Cancer Res. *25*, 3517–3527.

34. Miller, A., and Russell, S.J. (2016). The use of the NIS reporter gene for optimizing oncolytic virotherapy. Expert Opin. Biol. Ther. *16*, 15–32.

35. Chaurasiya, S., Chen, N.G., Lu, J., Martin, N., Shen, Y., Kim, S.I., Warner, S.G., Woo, Y., and Fong, Y. (2020). A chimeric poxvirus with J2R (thymidine kinase) deletion shows safety and anti-tumor activity in lung cancer models. Cancer Gene Ther. *27*, 125–135.

36. Chaurasiya, S., Yang, A., Kang, S., Lu, J., Kim, S.I., Park, A.K., Sivanandam, V., Zhang, Z., Woo, Y., Warner, S.G., and Fong, Y. (2020). Oncolytic poxvirus CF33-hNIS-ΔF14.5 favorably modulates tumor immune microenvironment and works synergistically with anti-PD-L1 antibody in a triple-negative breast cancer model. OncoImmunology *9*, 1729300.

37. O'Leary, M.P., Choi, A.H., Kim, S.I., Chaurasiya, S., Lu, J., Park, A.K., Woo, Y., Warner, S.G., Fong, Y., and Chen, N.G. (2018). Novel oncolytic chimeric orthopoxvirus causes regression of pancreatic cancer xenografts and exhibits abscopal effect at a single low dose. J. Transl. Med. *16*, 110.

38. Sherman, M.H., Yu, R.T., Engle, D.D., Ding, N., Atkins, A.R., Tiriac, H., Collisson, E.A., Connor, F., Van Dyke, T., Kozlov, S., et al. (2014). Vitamin D receptor-mediated stromal reprogramming suppresses pancreatitis and enhances pancreatic cancer therapy. Cell *159*, 80–93.

39. Woo, Y., Zhang, Z., Yang, A., Chaurasiya, S., Park, A.K., Lu, J., Kim, S.I., Warner, S.G., Von Hoff, D., and Fong, Y. (2020). Novel chimeric immuno-oncolytic virus CF33-hNIS-antiPDL1 for the treatment of pancreatic cancer. J. Am. Coll. Surg. *230*, 709–717.